21. Y. Wakatsuki, H. Yamazaki, N. Kumegawa, T. Satoh, J. Y. Satoh, *J. Am. Chem. Soc.* **113**, 9604 (1991).
22. Data collections were performed at 20°C on a Bruker SMART APEX diffractometer with a charge-coupled device (CCD) area detector, with graphite-monochromated Mo $K\alpha$ radiation (λ = 0.71073 Å). Molecular structures were solved by direct methods and refined on F^2 by full-matrix least-squares techniques. Monoclinic, $P2(1)/c$ (#14), a = 13.278 ± 0.005, b = 12.552 ± 0.005, c = 14.289 ± 0.006 (Å), β = 114.439 ± 0.008°, V = 2168.2 ± .15 Å^3, Z = 4, R = 0.0476, Rw = 0.0455. Crystallographic data were deposited in the Cambridge Crystallographic Database Centre (*trans*-**2a**: CCDC-175616; *trans*-**2b**: 175617).
23. L. Hagelee, R. West, J. Calabrese, J. Norman, *J. Am. Chem. Soc.* **101**, 4888 (1979).
24. D. Bright, O. S. Mills, *J. Chem. Soc. A* **1971**, 1979 (1971).
25. J. Yin, K. A. Abboud, W. M. Jones, *J. Am. Chem. Soc.* **115**, 8859 (1993).
26. V. Typke, J. Haase, A. Krebs, *J. Mol. Struct.* **56**, 77 (1979).
27. J. Haase, A. Krebs, *Z. Naturforsch.* **27a**, 624 (1972).
28. _____, *Z. Naturforsch.* **26a**, 1190 (1971).
29. F. H. Allen, *J. Chem. Soc. Perkin Trans. II* **1987**, S1 (1987).
30. H.-H. Bartsch, H. Colberg, A. Krebs, *Z. Kristallogr.* **156**, 10 (1981).
31. W. E. Hunter, D. C. Hrncir, R. V. Bynum, R. A. Penttila, J. L. Atwood, *Organometallics* **2**, 750 (1983).
32. U. Rosenthal *et al.*, *Z. Anorg. Allg. Chem.* **621**, 77 (1995).
33. C. Lefeber *et al.*, *J. Organomet. Chem.* **501**, 189 (1995).
34. W. Ahlers, B. Temme, G. Erker, R. Fröhlich, F. Zippel, *Organometallics* **16**, 1440 (1997).
35. J. Pflug, R. Fröhlich, G. Erker, *J. Chem. Soc. Dalton Trans.* **1999**, 2551 (1999).
36. H. Yasuda, Y. Kajihara, K. Mashima, K. Lee, A. Nakamura, *Chem. Lett.* **1980**, 519 (1980).
37. G. Erker, J. Wicher, K. Engel, F. Rosenfeldt, W. Dietrich, *J. Am. Chem. Soc.* **102**, 6344 (1980).
38. H. G. Alt, C. E. Denner, R. Zenk, *J. Organomet. Chem.* **433**, 107 (1992).
39. N. Suzuki *et al.*, *J. Organomet. Chem.* **473**, 117 (1994).
40. Heterolytic dissociation of a Zr-C bond might be possible as the mechanism for the isomerization. See E.-i. Negishi *et al.*, *J. Am. Chem. Soc.* **116**, 9751 (1994).
41. We sincerely thank K. Kobayashi (RIKEN) for assistance in x-ray diffraction analysis.

16 October 2001; accepted 13 December 2001

Hydrophobicity at a Janus Interface

Xueyan Zhang, Yingxi Zhu, Steve Granick

Water confined between adjoining hydrophobic and hydrophilic surfaces (a Janus interface) is found to form stable films of nanometer thickness whose responses to shear deformations are extraordinarily noisy. The power spectrum of this noise is quantified. In addition, the frequency dependence of the complex shear modulus is a power law with slope one-half, indicating a distribution of relaxation processes rather than any dominant one. The physical picture emerges that whereas surface energetics encourage water to dewet the hydrophobic side of the interface, the hydrophilic side constrains water to be present, resulting in a flickering, fluctuating complex.

The role of water as a solvent or lubricant in physical situations from biology to geology is almost universally thought to be important, but the details are disputed (*1–19*). In proteins, for example, the side chains of roughly half the amino acids are polar whereas the other half are hydrophobic; the nonmixing of the two is a major mechanism steering the folding of proteins and other self-assembly processes. Similarly, it is an everyday occurrence to observe the beading-up of raindrops, on raincoats or the leaves of plants. Moreover, it has been observed theoretically and experimentally that when the gap between two hydrophobic surfaces becomes critically small, water is spontaneously ejected (*10*, *15–19*), whereas water films confined between symmetric hydrophilic surfaces are stable at comparable spacings (*3*). It is then interesting to consider the antisymmetric situation, with a hydrophilic surface on one side to contain the water and a hydrophobic surface on the other to force it away. This Janus situation is shown in Fig. 1.

The main result of this experimental study is that when water is confined between these two competing tendencies, the result is neither simple wetting nor dewetting. We observe instead giant fluctuations (of the dynamical shear responses) around a well-defined mean. This noise and fluctuation are peculiar to water and are not observed with nonpolar fluids (*20*) or with a polar fluid such as ethanol. Aqueous films in the confined, symmetrically hydrophilic situation also give stable dynamical responses (*21*). The implied spatial scale of fluctuations is enormous compared to the size of a water molecule and lends support to the theoretical prediction that an ultrathin gas gap forms spontaneously when an extended hydrophobic surface is immersed in water (*5*, *10*, *12*).

The atomically smooth clay surfaces used in this study—muscovite mica (hydrophilic) and muscovite mica blanketed with a methyl-terminated organic self-assembled monolayer (SAM) (hydrophobic)—allowed the surface separation to be measured by multiple beam interferometry. Pairs of hydrophilic-hydrophobic surfaces were brought to the spacings described below by means of a surface forces apparatus (*3*) modified for dynamic oscillatory shear (*22*, *23*). A droplet of water was placed between the two surfaces oriented in crossed cylinder geometry. Piezoelectric bimorphs were used to produce and detect controlled shear motions. The deionized water was previously passed through a purification system, Barnstead Nanopure II (control experiments with water containing dissolved salt were similar). In experiments using degassed water, the water was either first boiled, then cooled in a sealed container, or was subjected to vacuum for 5 to 10 hours in an oven at room temperature. The temperature at which the measurements were taken was 25°C.

In order to firmly determine that the findings did not depend on the details of surface preparation, three methods were used to render one surface hydrophobic. In order of increasing complexity, these were (i) atomically smooth mica coated with a SAM of condensed octadecyltriethoxysiloxane (OTE), according to methods described previously (*23*); (ii) mica coated by means of Langmuir-Blodgett methods with a monolayer of condensed OTE; and (iii) a thin film of silver sputtered onto atomically smooth mica, then coated with a self-assembled thiol monolayer. In method (i), the monolayer quality was improved by distilling the OTE before self-assembly. In method (ii), OTE was spread onto aqueous HCl (pH, 2.5), 0.5 hour was allowed for hydrolysis, the film was slowly compressed to the surface pressure π = 20 mN m^{-1} (3 to 4 hours), and the close-packed film was transferred onto mica by the Langmuir-Blodgett technique at a creep-up speed of 2 mm min^{-1}. Finally the transferred films were vacuum-baked at 120°C for 2 hours. In method (iii), 650 Å of silver were sputtered at 1 Å s^{-1} onto mica that was held at room temperature, then octadecanethiol was deposited from 0.5 mM ethanol solution. In this case, atomic force microscopy (AFM) (with a Nanoscope II) showed the root mean square roughness to be 0.5 nm. All three methods led to the same conclusions. The contact angle of water with the hydrophobic surface was θ = 110° ± 2° (OTE surfaces) and θ = 120° ± 2° (octadecanethiol). In shear experiments, the sheared plate held the hydrophobic alkane monolayer.

The starting point was to measure the force-distance profile. The inset of Fig. 1 shows force, normalized by the mean radius of curvature of the crossed cylinders ($R \approx 2$ cm), plotted against surface separation (D). Each datum refers to an equilibration of 5 to 10 min. Attraction was observed starting at very large separations, $D \approx 0.5$ μm, and the slope of the ensuing

Department of Materials Science and Engineering, University of Illinois, Urbana, IL 61801, USA.

force-distance attraction was nearly proportional to the spring constant of the force-measuring spring. This indicated, according to well-known arguments (*3*), that the measurements represented points of instability at which the force gradient exceeded the spring constant of the force-measuring device, although these attractive forces were very slow to develop (*24*). The opposed surfaces ultimately sprang into contact from $D \approx 5$ nm and when the surfaces were pulled apart, an attractive minimum was observed at $D = 5.4$ nm. The surfaces could be squeezed to lesser thickness. Knowing that the linear dimension of a water molecule is ≈0.25 nm (*3*), the thickness of the resulting aqueous films amounted to on the order of 5 to 20 water molecules, although it is not clear that molecules were distributed evenly across this space.

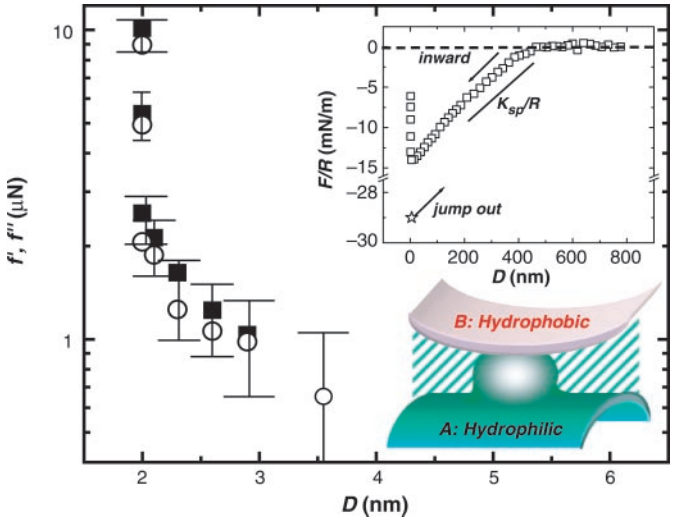

Fig. 1. Deionized water confined between a hydrophilic surface (A) on one side and a hydrophobic surface (B) on the other. The cartoon is not to scale, because the gap thickness is nanometers at closest approach and the droplet size (≈2 mm on a side) vastly exceeds the contact zone (≈10 μm on a side). The main figure shows the time-averaged viscous (circles) and elastic (squares) shear forces measured at 1.3 Hz and 0.3 nm deflection, plotted semi-logarithmically against surface separation for deionized water confined between OTE deposited onto mica by means of the Langmuir-Blodgett technique (shear impulses were applied to this hydrophobic surface). The inset shows the static force-distance relations. Force, normalized by the mean radius of curvature ($R \approx 2$ cm) of the crossed cylinders, is plotted against the thickness of the water film ($D = 0$ refers to contact in air) as the spacing was decreased. The pull-off adhesion at $D \approx 5.4$ nm is indicated by a star. The straight line with slope K_{sp}/R indicates the onset of a spring instability where the gradient of attractive force exceeds the spring constant (K_{sp}), 930 N m^{-1}. After this "jump" into contact, films of stable thickness resulted, whose thickness could be varied in the range $D = 1$ to 4 nm by the application of compressive force.

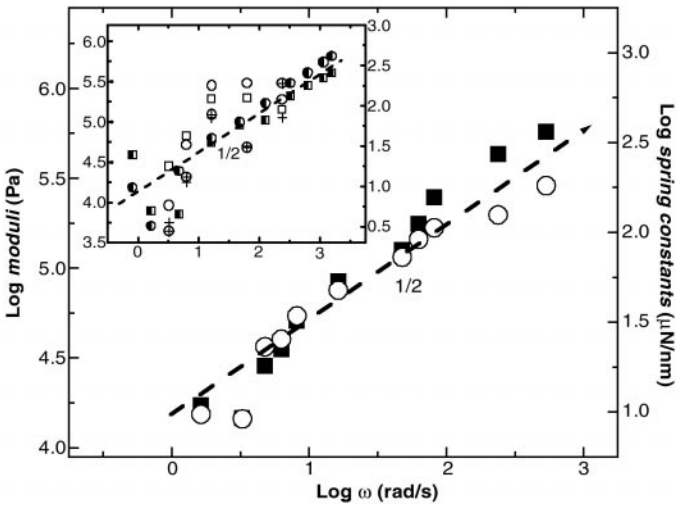

Fig. 2. For the situation depicted in Fig. 1, the frequency dependence of the momentum transfer between the moving surface (hydrophobic) and the aqueous film with adjoining stationary (hydrophilic) surface is plotted on log-log scales. Time-averaged quantities are plotted. On the right-hand ordinate scale are the viscous, g'' (circles), and elastic, g' (squares), spring constants. On the left-hand ordinate are the equivalent loss moduli, G_{eff}'' (circles), and elastic moduli, G_{eff}' (squares). All measurements were made just after the jump into contact shown in Fig. 1; that is, at nearly the same compressive pressure, ≈3 MPa. The main panel, representing Langmuir-Blodgett–deposited OTE, shows $\omega^{1/2}$ scaling after long-time averaging, 0.5 to 1 hour per datum. The inset shows comparisons with other methods used to produce a hydrophobic surface. In those experiments, the thickness was generally $D = 1.5$ to 1.6 nm but was occasionally as large as 2.5 nm when dealing with octadecanethiol monolayers. Symbols in the inset show data averaged over only 5 to 10 min with hydrophobic surfaces prepared with (i) a SAM of OTE (half-filled symbols), (ii) Langmuir-Blodgett deposition of OTE (crossed symbols), or (iii) deposition of octadecanethiol on Ag (open symbols). As in the main figure, circles denote viscous forces and squares denote elastic forces. Scatter in this data reflects shorter averaging times than in the main part of this figure (compare Fig. 3).

In our shear measurements, the sinusoidal shear deformations were gentle, the significance of the resulting linear response being that the act of measurement did not perturb the equilibrium structure (linear responses were verified from the absence of harmonics). Using techniques that are well known in rheology, from the phase lag and amplitude attenuation, these were decomposed into one component in phase (the elastic force, f') and one component out of phase (the viscous force, f'') (*25*). The main portion of Fig. 1 illustrates responses at a single frequency and variable thickness. The shear forces stiffened by more than an order of magnitude as the films were squeezed. When molecularly thin aqueous films are confined between clay surfaces that are symmetrically hydrophilic, deviations from the response of bulk water appear only at lesser separations (*21*); evidently the physical origin is different here. Moreover, at each separation, the elastic and viscous forces were nearly identical. Again, this contrasts with recent studies of molecularly thin water films between surfaces that are symmetrically hydrophilic (*21*). The equality of elastic and viscous forces proved to be general, not an accident of the shear frequency chosen.

Physically, these shear responses reflected the efficiency of momentum transfer between the moving (hydrophobic) surface and the adjoining water films. Figure 2 illustrates the unusual result that the in-phase and out-of-phase shear forces scaled in magnitude with the same power law: the square root of excitation frequency. This behavior, which is intermediate between "solid" and "liquid," is often associated in other systems with dynamical heterogeneity (*26*, *27*). According to known arguments, it indicates a broad distribution of relaxation times rather than any single dominant one. In Fig. 2, shear forces have been normalized in two alternative ways. The right-hand ordinate scale shows viscous and elastic forces with units of spring constant, force per nanometer of sinusoidal shear motion. Additional normalization for film thickness and estimated contact area gave the effective loss modulus $G_{eff}''(\omega)$, out of phase with the drive, and the elastic modulus $G_{eff}'(\omega)$ (left ordinate), in phase with the drive, where ω denotes radian frequency. The slope of 1/2 is required mathematically by the Kramers-Kronig relations if $G'(\omega) = G''(\omega)$ (*25*); its observation lends credibility to the measurements. The main portion of Fig. 2 illustrates this scaling for an experiment in which data were averaged over a long time. The inset shows that the same was observed when other methods were used to prepare a hydrophobic surface. In all of these instances, $\omega^{1/2}$ scaling was observed regardless of the method used to render the surface hydrophobic, but required extensive time averaging.

It is worth emphasizing that the magnitudes

of the shear moduli in Fig. 2 are "soft," something like those of agar or jelly. They were considerably softer than for molecularly thin aqueous films confined between surfaces that are symmetrically hydrophilic (*21*). In repeated measurements at the same frequency, we observed giant fluctuations around a definite mean, as illustrated in Fig. 3, A through C, although water confined between symmetric hydrophilic-hydrophilic surfaces (Fig. 3D) did not display this.

It is extraordinary that fluctuations did not average out over the large contact area (≈10 μm on a side) that far exceeded any molecular size. The structural implication is that the confined water film comprised some kind of fluctuating complex, seeking momentarily to dewet the hydrophobic side by a thermal fluctuation in one direction, but unable to do so because of the nearby hydrophilic side; seeking next to dewet the hydrophobic side by a thwarted fluctuation in another direction; and so on. Indeed, as Weissman emphasizes (*28*), nearby hydrophobic and hydrophilic surfaces may produce a quintessential instance of competing terms in the free energy, to satisfy which there may be many metastable states that are equally bad (or almost equally bad) compromises (*29*, *30*). This suggests the physical picture of flickering capillary-type waves, sketched hypothetically in Fig. 3E. These proposed long-wavelength capillary fluctuations would differ profoundly from those at the free liquid-gas interface, because they would be constricted by the nearby solid surface.

The possible role of dissolved gas is clear in the context of our proposed physical explanation. Indeed, submicrometer-sized bubbles resulting from dissolved air have been proposed to explain the anomalously long range of the hydrophobic attraction observed between extended surfaces (*15*–*19*) and have been visualized by AFM (*17*, *18*). To test this idea, first we performed control experiments using degassed water. The power spectrum (in Fig. 3F) was nearly the same. Although we cannot exclude the possibility that a small amount of residual dissolved gas was responsible, this method of degassing is reported to remove long-range hydrophobic attraction (*16*), whereas this comparison shows the consequence in the present situation to be minor. Next, we tested the idea that significant amounts of gas might remain adsorbed even in experiments with degassed water. The hydrophobic (SAM-coated) surface was first wetted with ethanol, and the absence of noisy shear response was verified. The ethanol was then flushed with copious amounts of degassed deionized water without exposing the surfaces to air. It was observed repeatedly that noisy responses to shear had reappeared when measurements were resumed after 30 min (Fig. 3A). We conclude that the effects reported in this paper did not stem from the presence of dissolved gas, although it is unclear why the fluctuations were even larger after ethanol rinse (Fig. 3A) than without it (Fig. 3B). Figure 3, A through D, illustrate the time-dependent viscous shear responses in various systems, with and without degassed water (see figure legend for details). Fluctuations of the elastic forces, not shown, followed the same pattern.

The power spectrum of this viscous response is shown in Fig. 3F. The power spectrum is the decomposition of the traces into their Fourier components, whose squared amplitudes are plotted, on log-log scales, against Fourier frequency. One observes, at very low Fourier frequencies, a high level of "white," frequency-independent noise. But the amplitude began to decrease beyond the Fourier frequency, $f \approx 0.001$ Hz, about 10^3 times less than the drive frequency. Other experiments (*31*) showed the same threshold Fourier frequency when the drive frequency was raised from 1.3 to 80 Hz, and therefore it appears to be a characteristic feature of the system. It defines a characteristic time for rearrangement of some kind of structure, $\approx 10^3/2\pi$ s; we tentatively identify this with the lifetime of bubble or vapor. The subsequent decay of the power spectrum as roughly $1/f^2$ suggests that these fluctuations reflect discrete entities, because smooth variations would decay more rapidly (*28*). Noise again appeared to become "white" but with amplitude 10^4 times smaller at $f > 0.1$ Hz, but the physical origin of this is not evident at this time. It did not reflect instrumental response, because the power spectrum for water confined between symmetrically hydrophilic surfaces was much less. Whether the fluctuations we observed were actually created by the drive or are also present at equilibrium has not been determined unequivocally, but the linearity of the shear moduli suggests the latter, and theoretical ideas support this (*10*, *12*). The noisy response appears to represent some collection of long-lived metastable configurations whose free energies are similar.

From recent theoretical analysis of the hydrophobic interaction, the expectation of dewetting emerges: it is predicted that an ultrathin gas gap, with thickness on the order of 1 nm, forms spontaneously when an extended hydrophobic surface is immersed in water (*5*, *10*, *12*). The resulting capillary wave spectrum does not appear to have yet been considered theoretically, but for the related case of the free water-vapor interface, measurements confirm that capillary waves with a broad spectrum of wavelengths up to micrometers in size contribute to

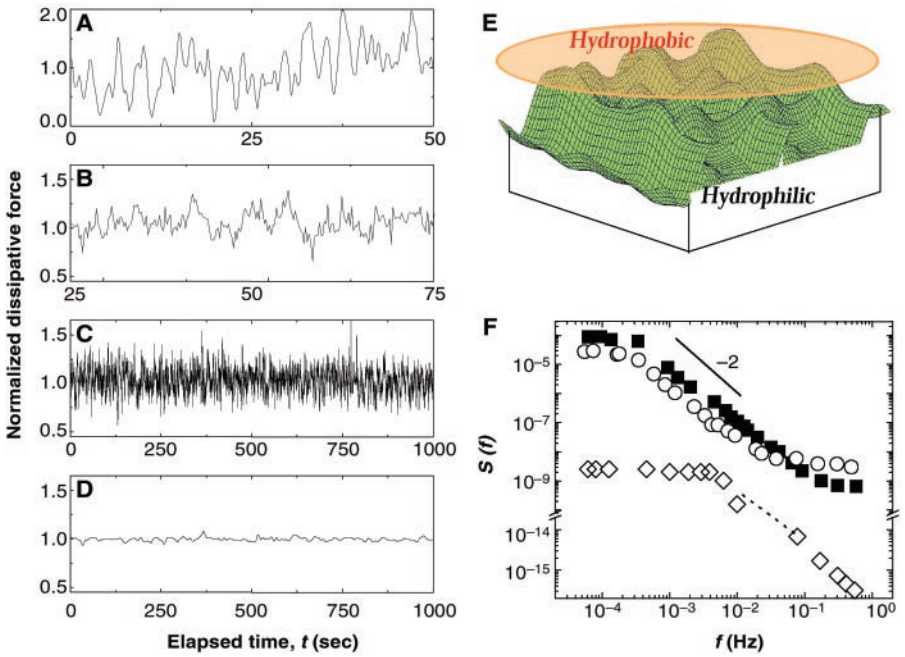

Fig. 3. The prominence of fluctuations for water confined in a Janus interface is illustrated. In (A) through (C), the viscous forces, normalized to the mean (at 1.3 Hz), are plotted against time elapsed. In (**A**), the surfaces were first wet with ethanol to remove adsorbed gas, then flushed with degassed deionized water. In (**B**), the ethanol rinse was omitted, and the water was not degassed. (**C**) shows a long time trace for data taken under the same conditions as for (B). (**D**) illustrates that deionized water confined between symmetric hydrophilic-hydrophilic surfaces did not display noisy responses. Confined ethanol films likewise failed to display noisy responses (not shown in the figure). (**F**) shows the power spectrum for deionized water and the hydrophobized surface composed of OTE deposited by the Langmuir-Blodgett technique (squares); degassed deionized water and the hydrophobized surface composed of an octadecanethiol monolayer (circles); and water containing 25 mM NaCl confined between symmetric hydrophilic-hydrophilic surfaces (diamonds). To calculate the power spectra, the time elapsed was at least 10^5 s (the complete time series is not shown). The power-law exponent is close to −2. (**E**) shows a proposed explanation: the capillary waves of water meeting the hydrophobic surface with a flickering vapor phase in between.

its width (*32*). On physical grounds, the thin gas gap suggested by our measurements should also be expected to possess soft modes with fluctuations whose wavelength ranges from small to large. From this perspective, we then expect that the experimental geometry of a Janus-type water film, selected for experimental convenience, was incidental to the main physical effect.

These conclusions have evident connections to understanding the long-standing question of the structure of aqueous films near a hydrophobic surface and may have a bearing on understanding the structure of water films near the patchy hydrophilic-hydrophobic surfaces that are so ubiquitous in nature.

Note added in proof: We have recently been made aware of neutron reflectivity experiments that indicate the existence of a nanometer-thick vapor-like coating that forms on an extended hydrophobic surface when it is immersed in water (*33, 34*).

References and Notes

1. W. Kauzmann, *Adv. Prot. Chem.* **14**, 1 (1959).
2. C. Tanford, *The Hydrophobic Effect–Formation of Micelles and Biological Membranes* (Wiley-Interscience, New York, 1973).
3. J. N. Israelachvili, *Intermolecular and Surface Forces* (Academic Press, New York, ed. 2, 1991).
4. F. H. Stillinger, *J. Solution Chem.* **2**, 141 (1973).
5. E. Ruckinstein, P. Rajora, *J. Colloid Interface Sci.* **96**, 488 (1983).
6. L. R. Pratt, D. Chandler, *J. Chem. Phys.* **67**, 3683 (1977).
7. A. Ben-Naim, *Hydrophobic Interaction* (Kluwer Academic/Plenum, New York, 1980).
8. A. Wallqvist, B. J. Berne, *J. Phys. Chem.* **99**, 2893 (1995).
9. G. Hummer, S. Garde, A. E. Garcia, A. Pohorille, L. R. Pratt, *Proc. Natl. Acad. Sci. U.S.A.* **93**, 8951 (1996).
10. K. Lum, D. Chandler, J. D. Weeks, *J. Phys. Chem. B* **103**, 4570 (1999).
11. Y. K. Cheng, P. J. Rossky, *Biopolymers* **50**, 742 (1999).
12. D. M. Huang, D. Chandler, *Proc. Natl. Acad. Sci. U.S.A.* **97**, 8324 (2000).
13. G. Hummer, S. Garde, A. E. Garcia, L. R. Pratt, *Chem. Phys.* **258**, 349 (2000).
14. D. Bratko, R. A. Curtis, H. W. Blanch, J. M. Prausnitz, *J. Chem. Phys.* **115**, 3873 (2001).
15. Y.-H. Tsao, D. F. Evans, H. Wennerström, *Science* **262**, 547 (1993) and references therein.
16. R. F. Considine, C. J. Drummond, *Langmuir* **16**, 631 (2000).
17. N. Ishida, T. Inoue, M. Miyahara, K. Higashitani, K. Higashitani, *Langmuir* **16**, 6377 (2000).
18. J. W. G. Tyrrell, P. Attard, *Phys. Rev. Lett.* **87**, 176104 (2001).
19. X. Zhang, Y. Zhu, S. Granick, *J. Am. Chem. Soc.* **123**, 6736 (2001).
20. J. Peanasky, L. Cai, C. R. Kessel, S. Granick, *Langmuir* **10**, 3874 (1994).
21. Y. Zhu, S. Granick, *Phys. Rev. Lett.* **87**, 096104 (2001).
22. J. Peachey, J. Van Alsten, S. Granick, *Rev. Sci. Instrum.* **62**, 463 (1991).
23. J. Peanasky, H. M. Schneider, C. R. Kessel, S. Granick, *Langmuir* **11**, 953 (1995).
24. As reviewed by E. Kokkoli and C. F. Zukoski [*J. Colloid Interface Sci.* **230**, 176 (2000)], equilibrium force-distance interactions between opposed hydrophobic and hydrophilic surfaces have also been studied, in other systems, by other researchers.
25. J. D. Ferry, *Viscoelastic Properties of Polymers* (Wiley, New York, ed. 3, 1982).
26. H. H. Winter, F. Chambon, *J. Rheol.* **30**, 367 (1986).
27. R. Yamamoto, A. Onuki, *Phys. Rev. E* **58**, 3515 (1998) and references therein.
28. M. B. Weissman, personal communication.
29. A. O. Parry, R. Evans, *Phys. Rev. Lett.* **64**, 439 (1990)
30. K. Binder, D. P. Landau, A. M. Ferrenberg, *Phys. Rev. E* **51**, 2823 (1995).
31. X. Zhang, Y. Zhu, S. Granick, data not shown.
32. D. K. Schwartz *et al.*, *Phys. Rev. A* **41**, 5687 (1990).
33. M. Grünze, personal communication.
34. R. K. Thomas, personal communication.

35. We thank H. Lee for performing the control experiment with ethanol rinse and D. Chandler, J. F. Douglas, and M. B. Weissman for invaluable discussions. Supported by the U.S. Department of Energy, Division of Materials Science, under award number DEFG02-91ER45439 to the Frederick Seitz Materials Research Laboratory at the University of Illinois at Urbana-Champaign.

10 September 2001; accepted 12 December 2001

Beta-Diversity in Tropical Forest Trees

Richard Condit,[1]* Nigel Pitman,[2] Egbert G. Leigh Jr.,[1] Jérôme Chave,[3] John Terborgh,[2] Robin B. Foster,[4] Percy Núñez V.,[5] Salomón Aguilar,[1] Renato Valencia,[6] Gorky Villa,[6] Helene C. Muller-Landau,[7] Elizabeth Losos,[8] Stephen P. Hubbell[9]

The high alpha-diversity of tropical forests has been amply documented, but beta-diversity—how species composition changes with distance—has seldom been studied. We present quantitative estimates of beta-diversity for tropical trees by comparing species composition of plots in lowland terra firme forest in Panama, Ecuador, and Peru. We compare observations with predictions derived from a neutral model in which habitat is uniform and only dispersal and speciation influence species turnover. We find that beta-diversity is higher in Panama than in western Amazonia and that patterns in both areas are inconsistent with the neutral model. In Panama, habitat variation appears to increase species turnover relative to Amazonia, where unexpectedly low turnover over great distances suggests that population densities of some species are bounded by as yet unidentified processes. At intermediate scales in both regions, observations can be matched by theory, suggesting that dispersal limitation, with speciation, influences species turnover.

Beta-diversity is central to concepts about what controls diversity in ecological communities. Species turnover can reflect deterministic processes, such as species' adaptations to differences in climate or substrate, or it can result from limited dispersal coupled with speciation, delayed response to climatic change, or other historical effects. Perhaps more important, beta-diversity is as important as alpha-diversity for conservation, because species turnover influences diversity at large scales. Recently, Hubbell (*1*) and Harte *et al.* (*2*, *3*) have derived theories relating species turnover with distance to species-area relations and total species richness. In very rich forests of the neotropics, these theories may allow us to interpolate species turnover and estimate species distributions and diversity at scales relevant to conservation even with the sparse data from forest plots that are currently available.

To measure beta-diversity and test factors influencing it, we identified all trees in 34 plots near the Panama Canal, 16 plots in Ecuador's Yasuní National Park, and 14 plots in Peru's Manu Biosphere Reserve (*4*–*7*). All plots were in terra firme, or unflooded, forests. Over 50,000 trees ≥10-cm stem diameter were tagged, measured, and sorted to morphospecies. The similarity between two plots was measured three different ways: Sørensen's and Jaccard's measures of the fraction of species shared and the probability F that two trees chosen randomly, one from each plot, are the same species (*8*). The Sørensen and Jaccard indices weight all species equally; F is influenced primarily by common species. We used the overall decay of similarity in species composition with distance as a measure of beta-diversity (*9*).

[1]Center for Tropical Forest Science, Smithsonian Tropical Research Institute, Unit 0948, APO AA 34002–0948, USA. [2]Center for Tropical Conservation, Duke University, Box 90381, Durham, NC 27708–0381, USA. [3]Laboratoire d'Ecologie Terrestre, CNRS, UMR 5552, 12 avenue du Colonel Roche, BP4072, 31029 Toulouse, France. [4]Botany Department, The Field Museum, Roosevelt Road at Lake Shore Drive, Chicago, IL 60605–2496, USA. [5]Herbario Vargas, Universidad Nacional San Antonio de Abad, Cusco, Peru. [6]Department of Biological Sciences, Pontificia Universidad Catolica del Ecuador, Apartado 17-01-2184, Quito, Ecuador. [7]Department of Ecology and Evolutionary Biology, Princeton University, Princeton, NJ 08544, USA. [8]Center for Tropical Forest Science, Smithsonian Institution, 900 Jefferson Drive, Suite 2207, Washington, DC 20560, USA. [9]Department of Botany, University of Georgia, Athens, GA 30602, USA.

*To whom correspondence should be addressed.